JVI Journals.ASM.org

1918 Influenza Virus Hemagglutinin (HA) and the Viral RNA Polymerase Complex Enhance Viral Pathogenicity, but Only HA Induces Aberrant Host Responses in Mice

Tokiko Watanabe,[a,b] Jennifer Tisoncik-Go,[c] Nicolas Tchitchek,[c] Shinji Watanabe,[a,b] Arndt G. Benecke,[c,d] Michael G. Katze,[c] Yoshihiro Kawaoka[a,b,e,f]

Department of Pathobiological Sciences, School of Veterinary Medicine, University of Wisconsin—Madison, Madison, Wisconsin, USA[a]; ERATO Infection-Induced Host Responses Project, Japan Science and Technology Agency, Saitama, Japan[b]; Department of Microbiology, School of Medicine, University of Washington, Seattle, Washington, USA[c]; Université Pierre et Marie Curie, Centre National de la Recherche Scientifique, UMR7224, Paris, France[d]; Division of Virology, Department of Microbiology and Immunology, Institute of Medical Science, University of Tokyo, Tokyo, Japan[e]; Department of Special Pathogens, International Research Center for Infectious Diseases, Institute of Medical Science, University of Tokyo, Tokyo, Japan[f]

The 1918 pandemic influenza virus was the most devastating infectious agent in human history, causing fatal pneumonia and an estimated 20 to 50 million deaths worldwide. Previous studies indicated a prominent role of the hemagglutinin (HA) gene in efficient replication and high virulence of the 1918 virus in mice. It is, however, still unclear whether the high replication ability or the 1918 influenza virus HA gene is required for 1918 virus to exhibit high virulence in mice. Here, we examined the biological properties of reassortant viruses between the 1918 virus and a contemporary human H1N1 virus (A/Kawasaki/173/2001 [K173]) in a mouse model. In addition to the 1918 influenza virus HA, we demonstrated the role of the viral RNA replication complex in efficient replication of viruses in mouse lungs, whereas only the HA gene is responsible for lethality in mice. Global gene expression profiling of infected mouse lungs revealed that the 1918 influenza virus HA was sufficient to induce transcriptional changes similar to those induced by the 1918 virus, despite difference in lymphocyte gene expression. Increased expression of genes associated with the acute-phase response and the protein ubiquitination pathway were enriched during infections with the 1918 and 1918HA/K173 viruses, whereas reassortant viruses bearing the 1918 viral RNA polymerase complex induced transcriptional changes similar to those seen with the K173 virus. Taken together, these data suggest that HA and the viral RNA polymerase complex are critical determinants of Spanish influenza pathogenesis, but only HA, and not the viral RNA polymerase complex and NP, is responsible for extreme host responses observed in mice infected with the 1918 influenza virus.

The 1918 influenza pandemic was one of the most deadly contagious calamities in human history. In 1918-1919, approximately 30% of the world's population (500 million people) may have been clinically infected (1), and the disease was unprecedentedly severe, with over 2.5% mortality rates among infected people, compared with less than 0.1% in annual influenza epidemics (1–3). The 1918 pandemic particularly attacked a young adult group that usually has a very low influenza death rate, resulting in more than 20-times-higher death rates from influenza and pneumonia for 15- to 34-year-olds in 1918 than in a previous year (1, 4). The majority of deaths were from secondary bacterial pneumonia due to the lack of antibiotics (1). However, the virus also killed people without bacterial infections, often with either massive acute pulmonary hemorrhage or pulmonary edema and frequently in less than 5 days (1, 5–7).

The reconstructed 1918 virus caused a highly pathogenic respiratory infection in mice (8) and macaque models that culminated in acute respiratory distress and a fatal outcome (9). We and others have found that the hemagglutinin (HA) gene contributes to efficient viral replication and high virulence of the 1918 virus in mice (8, 10–12). In general, pathogenicity of virus in animals is thought to be associated with the ability of the virus to replicate in the respective hosts. Indeed, in the case of highly pathogenic H5N1 influenza viruses, an amino acid substitution (Glu to Lys) at position 627 in viral polymerase component, PB2, confers the high growth ability in mammalian cells to avian viruses, subsequently leading to increased pathogenicity of H5N1 virus in mammals (13–15). Pappas and colleagues recently showed a role for the 1918 virus HA and NA genes in efficient replication and pathogenicity in mice, suggesting a correlation between the efficient replication of the 1918 recombinant viruses in mouse lungs and the high virulence observed in mice (11). In their study, however, the 1918 virus HA gene was the only gene which was able to confer the property of high growth rate in mouse lungs to the contemporary human H1N1 virus (A/Texas/36/1991 [referred to here as Tx91]) (11). Although they also suggested the role of the 1918 virus PB1 gene in efficient replication in mice, the lung titer of a virus possessing the 1918 virus PB1 gene was 3 log units lower than that of a virus possessing the 1918 virus HA gene (11). Therefore, it was still unclear whether a high replication ability or the 1918 virus HA gene is required for 1918 virus to exhibit high virulence in mice.

To address this, here we examined replicative ability and pathogenicity of reassortant viruses between the 1918 virus and a contemporary human H1N1 virus (A/Kawasaki/173/2001

Received 5 October 2012 **Accepted** 21 February 2013
Published ahead of print 28 February 2013
Address correspondence to Tokiko Watanabe, twatanabe@svm.vetmed.wisc.edu, or Yoshihiro Kawaoka, kawaokay@svm.vetmed.wisc.edu.
T.W. and J.T.-G. contributed equally to this article.

doi:10.1128/JVI.02753-12

[K173]) in mice. We also performed transcriptional profiling of genes expressed in lungs of mice infected with reassortant viruses by microarray analysis.

MATERIALS AND METHODS

Cells. 293T human embryonic kidney cells and Madin-Darby canine kidney (MDCK) cells were maintained in Dulbecco's modified Eagle's medium supplemented with 10% fetal calf serum and in minimal essential medium (MEM) containing 5% newborn calf serum, respectively. All cells were maintained at 37°C in 5% CO_2.

Plasmid-driven reverse genetics. All reassortant viruses and parental 1918 and K173 viruses were generated by the introduction of plasmids expressing the respective eight viral RNA segments and three polymerase proteins plus NP into 293T cells, as described by Neumann et al. (16). Forty-eight hours posttransfection, viruses were harvested and used to inoculate MDCK cells for the production of stock viruses. Eight genes of each transfectant virus were partially sequenced to confirm the origin of the gene. All experiments with live viruses and with transfectants generated by reverse genetics were performed in a biosafety level 3 (BSL3) containment laboratory approved for such use by the CDC and the U.S. Department of Agriculture. The research program, procedures, occupational health plan, documentation, security, and facilities are reviewed annually by the University of Wisconsin—Madison responsible official and at regular intervals by the CDC and the Animal and Plant Health Inspection Service (APHIS) as part of the University of Wisconsin—Madison Select Agent Program.

Mouse experiments. Five- to six-week-old female BALB/c mice (The Jackson Laboratory) were used for the experiments. Isoflurane-anesthetized mice were intranasally inoculated with 10-fold serial dilutions (three mice per dilution) of viruses. The mice were monitored daily for 14 days for disease symptoms and survival. The dose required to kill 50% of mice (MLD_{50}) was calculated by the method of Reed and Muench (17). To determine the extent of viral replication in mice, we intranasally inoculated animals with 10^4 or 10^6 PFU of virus. At various time points after infection, organs were collected from the infected mice. The organs were homogenized, and virus titers were determined by plaque assay on MDCK cells.

Statistical analysis. Statistical analyses for virus lung titers and body weight changes in the infected mice were performed by using analysis of variance (ANOVA) in GraphPad Prism version 5.0 (GraphPad Software, Inc., La Jolla, CA); P values of <0.05 were considered significant.

Pathological examination. Mice infected with either the K173, 1918HA/K173, 1918PB1/K173, 1918(3P+NP)/173, or 1918 virus were euthanized at day 5 postinfection (p.i.) for pathological examination. Excised tissues of the lungs were preserved in 10% phosphate-buffered formalin. Tissues were then processed for paraffin embedding and cut into 5-μm-thick sections. One section was stained with routine hematoxylin and eosin (H&E), and the other was processed for immunohistological staining by using a rabbit anti-H1N1 influenza virus polyclonal antibody (anti-A/WSN/33) that was described and used elsewhere (9). Specific antigen-antibody reactions were visualized by 3,3′-diaminobenzidine tetrahydrochloride using a Dako EnVision system (Dako Co. Ltd., Tokyo, Japan).

Microarray experiments. Mice were intranasally inoculated with 10^6 PFU of virus ($n = 45$) or inoculated with phosphate-buffered saline ($n = 6$), and whole lungs were collected on days 1, 3, and 5 p.i. from infected animals (3/time point/group) and from control animals (2/time point) for microarray analysis. Two of three mice infected with either 1918 virus or 1918HA/K173 virus died by day 5 p.i. RNA was isolated from total lung homogenates, and fluorescently labeled probes were generated from each sample using an Agilent one-color low-input Quick Amp labeling kit (Agilent Technologies). Individual cRNA samples were hybridized to oligonucleotide microarrays for gene expression profiling using a whole-mouse-genome microarray kit (G4122A; Agilent Technologies), as previously described (18). RNA isolated from control animal lungs served as an uninfected reference. Quantitative reverse transcription-PCR was performed on mouse lung samples using a primer-probe set targeting the viral M sequence. A single biological replicate infected with 1918PB1/K173 virus at day 3 p.i. was confirmed to be uninfected, and the sample was discarded from the data set prior to analysis.

Data processing and normalization. Microarray raw data were extracted using the R bioconductor Limma package (19) and median normalized. The NeONORM normalization method (20) was used for interassay comparisons. Technical replicates were merged by averaging the means of the signals, weighted by their coefficient of variation.

Statistical analysis of microarray data. Differentially expressed genes were identified using the fold-change-based concomitant evaluation of distinctness and similarity (CDS) statistical test (21) with a fold-change (FC) parameter of 1.2 and a P value cutoff of <0.01.

Hierarchical clustering and SVD-MDS representations. Hierarchical clustering based on intensity data was performed using correlation metric and using the unweighted pair group method with arithmetic mean (UPGMA) agglomerative method. Singular value decomposition-multidimensional scaling (SVD-MDS) representations were obtained using the SVD-MDS method (22). The mathematical term correspondence space denotes a distance metric based on correspondence analysis that is used in data dimensionality reduction (44). The Kruskal stress represents the amount of information lost due to the dimensionality reduction as a fraction of total information (23).

Functional analysis of differential gene expression data. Data were analyzed through the use of IPA software (Ingenuity Systems, Inc.). This software examines RNA expression data in the context of known biological functions and pathways, mapping each gene identifier in a data set to its corresponding molecule in the Ingenuity Pathways Knowledge Base (IPKB). For all analyses, IPA-generated P values were adjusted using the Benjamini-Hochberg multiple testing correction to rank the significance for canonical pathways assigned to the data set. Pathway analysis diagrams show the biological associations among genes, represented as nodes, and the edges that define the biological relationship between two nodes, represented as a line. Solid lines depict direct interactions, and dashed lines depict indirect interactions. All edges are supported by at least one published reference or from canonical information stored in the IPKB. An arrow pointing between nodes signifies regulation, and an arrow pointing back to the same node signifies self-regulation.

Microarray data accession numbers. Primary microarray data have been deposited in NCBI's Gene Expression Omnibus (24) under GEO series accession number GSE44595 and are also available at the University of Washington's Public Microarray Data Download site (http://expression.microslu.washington.edu) and at the Institut des Hautes Etudes Scientifiques Public Mace Database (http://mace.ihes.fr, using accession number 2987824518).

RESULTS

Replicative properties of reassortant viruses between 1918 and contemporary human H1N1 viruses in mice. Previously, we and others demonstrated that the HA gene is essential for maximal viral replication and increased virulence of 1918 virus in mice (8, 10–12). To better understand the contribution of other viral genes to replicative ability and virulence of the 1918 virus in mice, we characterized reassortant viruses between the 1918 virus and a contemporary human H1N1 virus (A/Kawasaki/173/2001 [K173]) in mice. Mice were inoculated with 10^4 PFU of virus intranasally, and lung tissues were collected from the infected mice for virus titration at day 3 postinfection (p.i.). As shown in Table 1, virus titers in the lungs of mice infected with viruses possessing the 1918 PB1 or HA gene (designated 1918PB1/K173 and 1918HA/K173, respectively) exceeded 10^6 PFU/g, approximately 100-fold higher than those in mice infected with K173 virus ($P < 0.05$), suggesting that the PB1 and HA genes appear to

TABLE 1 Biological properties of reassortant viruses between the 1918 virus and a contemporary human H1N1 virus in mice

Virus	MLD_{50} (log_{10} PFU)	Virus titer in lungs (log_{10} PFU/g, mean ± SD)[a]
1918 WT	3.2	7.6 ± 0.8*
K173 WT	>6.5	4.6 ± 0.3
1918(3P+NP)/K173	>6.5	7.1 ± 0.5*
K173(3P+NP)/1918	6.1	4.5 ± 0.5
1918PA/K173	>6.5	4.5 ± 0.3
1918PB1/K173	>6.5	6.4 ± 0.6*
1918PB2/K173	>6.5	5.3 ± 0.7
1918NP/K173	>6.5	4.9 ± 0.1
1918HA/K173	4.8	6.2 ± 0.2*
1918NA/K173	>6.5	2.5 ± 0.3
1918M/K173	>6.5	5.3 ± 0.3
1918NS/K173	>6.5	3.2, 2.9

[a] BALB/c mice, anesthetized with isoflurane, were infected intranasally with 10^4 PFU of virus/50 μl. Three mice from each group were euthanized at day 3 postinfection for virus titration. When virus was not recovered from all three mice, individual titers were recorded. *, significantly different ($P < 0.05$) from the K173 virus titer as determined by the Student *t* test.

support efficient replication of the 1918 virus in mouse lungs, as reported previously (10, 11).

We next assessed the growth property of a virus possessing genes for the three 1918 virus polymerases, the PA, PB1, PB2, and NP genes [1918(3P+NP)/K173], in mouse lungs and found that the resultant viral titer was about 10-fold higher than the 1918PB1/K173 and 1918HA/K173 viral titers, which were essentially comparable to those of the 1918 virus (Table 1); there was, however, no statistical difference between the virus titers of 1918PB1/K173 and 1918HA/K173 and those of 1918(3P+NP)/K173. These data showed that 1918(3P+NP)/K173 virus by itself has the ability to replicate well in mouse lungs to the same extent as the 1918 virus without contribution from the 1918 virus HA, suggesting a prominent role for the 1918 polymerase complex in efficient virus growth in mice. Interestingly, the K173(3P+NP)/1918 virus achieved a lung titer that was similar to that of the K173 virus, despite possessing the 1918 virus HA gene (Table 1). We speculate that the K173(3P+NP)/1918 virus may be attenuated due to incompatibility between the 1918 and K173 viral proteins. Alternatively, the 1918 NA and/or NS genes may attenuate the K173(3P+NP)/1918 virus, given that reassortant viruses containing the 1918 virus NA or NS gene replicated less efficiently than did the K173 virus in mice (Table 1).

We further examined growth kinetics of the viruses whose lung titers were significantly higher than those of K173 virus in mice [i.e., 1918WT, 1918HA/K173, 1918PB1/K173, and 1918(3P+NP)/K173, as shown in Table 1]. Mice were intranasally inoculated with a high dose (10^6 PFU/50 μl) of viruses, and lung titers were determined at days 1, 3, and 5 p.i. The 1918 and 1918HA/K173 viruses replicated well throughout the infection, and the mean titers of both viruses were more than 10^7 PFU/g, whereas the replication of K173 virus was limited in mouse lungs (Fig. 1A). Although the titers of 1918PB1/K173 virus were significantly higher than those of K173 virus at days 1 and 5 p.i. ($P < 0.001$ and $P < 0.05$, respectively), this virus replicated less efficiently than 1918 virus did ($P < 0.01$ at all time points tested). Interestingly, 1918(3P+NP)/K173 virus grew well to the same extent as 1918 and 1918HA/K173 viruses at an early time point (day 1 p.i.); however, the titers of this virus declined at days 3 and 5 p.i., resulting in titers significantly lower than those of 1918 virus ($P < 0.001$ and $P < 0.01$ at days 3 and 5 p.i., respectively).

These results suggest that both 1918(3P+NP)/K173 and 1918HA/K173 viruses have the ability to replicate efficiently in mouse lungs to the same extent as 1918 virus at early time points in infection, whereas the 1918(3P+NP)/K173 virus, unlike 1918HA/K173 virus, which showed sustained viral replication in the course of infection, had started being cleared from mouse lungs at later time points.

Pathogenicity of reassortant viruses between 1918 and K173 viruses in mice. To examine the pathogenicity of reassortant viruses in mice, we next determined the MLD_{50} (amount of virus required to kill 50% of infected mice) and body weight changes of mice infected with a high dose (10^6 PFU) of viruses. The MLD_{50} for the 1918 virus was 3.2 log_{10} PFU (Table 1), and mice infected with 10^6 PFU of this virus showed severe weight loss and succumbed to infection as early as 4 days p.i. (Fig. 1B), underscoring its extraordinary virulence in a mouse model (8). The body weights of mice infected with 10^6 PFU of 1918HA/K173 virus decreased rapidly, and all of the infected mice died by day 7 p.i. (Fig. 1B) ($MLD_{50} = 4.8$ log_{10} PFU). Unlike the 1918 and 1918HA/K173 viruses, 1918(3P+NP)/K173 virus did not kill mice even at the highest dose tested, 8.4×10^7 PFU/mouse, while inoculation with 10^6 PFU of this virus did not lead to appreciable changes in

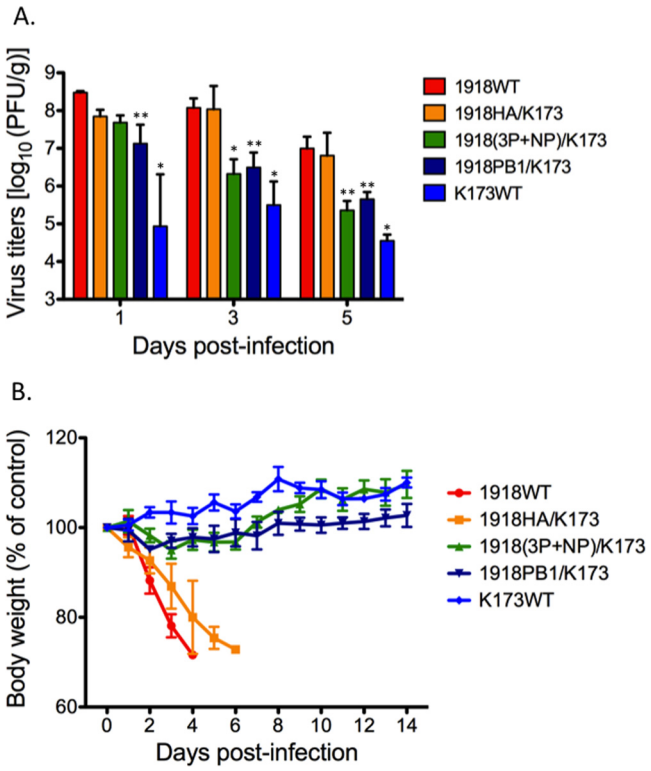

FIG 1 Pathogenicity of reassortant viruses in mice. Mice were intranasally infected with 10^6 PFU of each reassortant, 1918 virus, or K173 virus. (A) Lung tissues were collected from mice ($n = 3$) on the indicated days postinfection, and titers were determined in MDCK cells. Bars show the mean titers in lungs of the infected mice for the respective virus. Asterisks indicate that the mean titers of the respective virus were significantly lower than those of 1918 virus (*, $P < 0.001$; **, $P < 0.01$). (B) The body weights of the infected mice were monitored for 14 days. Mean changes in body weight are shown.

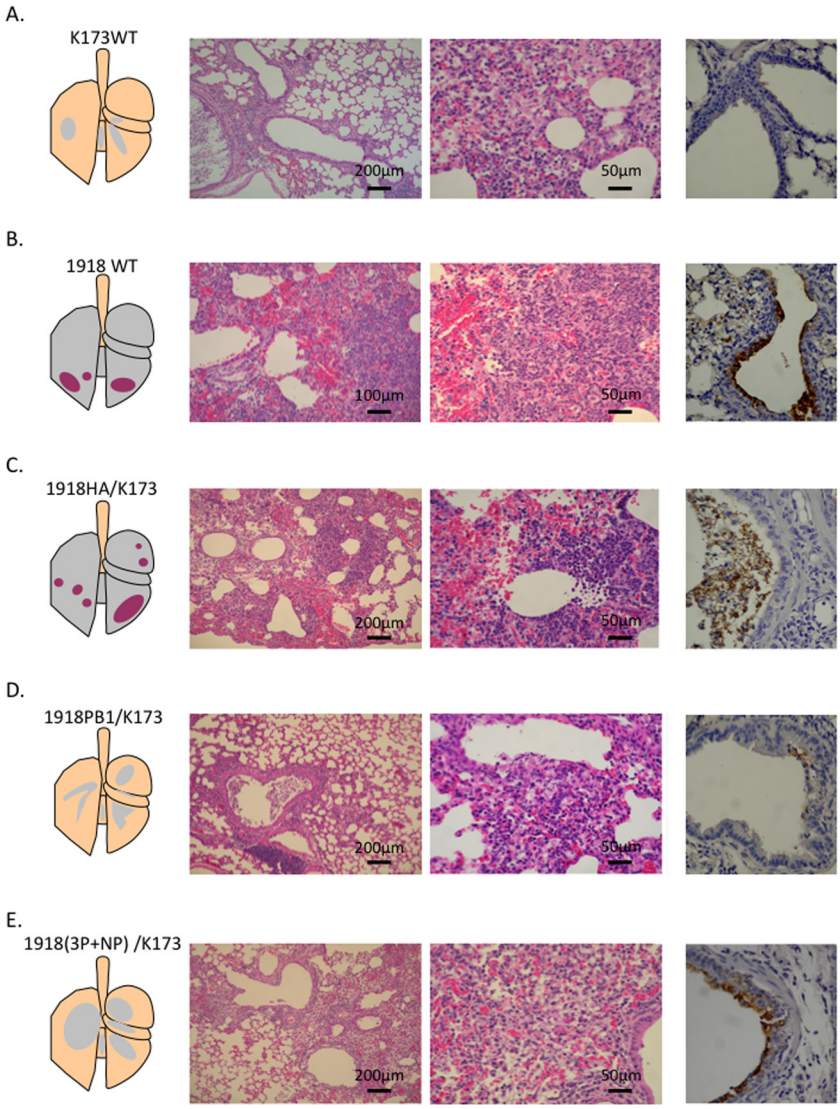

FIG 2 Pathological examination of lungs of mice infected with the indicated reassortant viruses at day 5 postinfection. Representative findings are shown to depict the distribution of lesions in the lung tissue sections (shown as sections placed next to the illustrations of lung), as follows: gray, inflammatory lesions containing viral-antigen-positive cells; violet, accumulation of neutrophils. The left and middle panels show lung sections with H&E staining, whereas the right panels show immunostaining with a rabbit anti-H1N1 influenza virus polyclonal antibody (anti-A/WSN/33) that was characterized previously (9). Global severe inflammatory reactions were prominent in the lungs of mice infected with 1918 or 1918HA/K173 virus. Viral antigens were distributed throughout the lung of mice infected with those viruses. Numerous neutrophilic infiltrations were prominent in the peribronchial area and alveolar wall. Hemorrhage and edematous lesions were observed (B and C, left and middle). In contrast, infection with K173, 1918PB1/K173, or 1918(3P+NP)/K173 virus produced only small, irregularly distributed inflammatory lesions in the mouse lungs (A, D, and E, left and middle). Lungs from the mice infected with 1918, 1918HA/K173, and 1918(3P+NP)/K173 viruses had viral antigen commonly found in bronchial lumina and alveoli (B, C, and E, right). Viral antigen in necrotic cellular debris was observed in the lungs of mice infected with 1918HA/K173 virus (C, right).

body weight (Fig. 1B). In contrast, despite its poor replication in mouse lungs (Table 1), K173(3P+NP)/1918 virus showed higher virulence than other reassortant viruses (presumably because of the 1918 virus HA gene), as judged from the MLD_{50} (Table 1). These results suggest that the 1918 virus HA gene contributes to both efficient replication and high virulence in mice, whereas the contribution of the polymerase and NP of 1918 virus appears to be limited to efficient viral replication in mouse lungs.

We performed pathological examination of lungs from mice infected with the reassortant viruses (Fig. 2). As demonstrated in previous studies (10, 25), infection with viruses possessing the 1918 virus HA gene (i.e., 1918 and 1918HA/K173 viruses) caused massive recruitment of polymorphonuclear cells (mainly neutrophils) accompanied by intra-alveolar hemorrhage (Fig. 2B and C). In contrast, mice infected with 1918(3P+NP)/K173 and 1918PB1/K173 viruses produced limited inflammatory foci that resulted from initial infection of the bronchioli with only minor extensions into the adjacent alveoli (Fig. 2D and E). Most of the lung had an appearance similar to that of the K173-infected mouse lungs (Fig. 2A). Lungs from the mice infected with 1918, 1918HA/K173, and 1918(3P+NP)/K173 viruses had viral antigen commonly found in bronchial lumina and alveoli (Fig. 2B, C, and E).

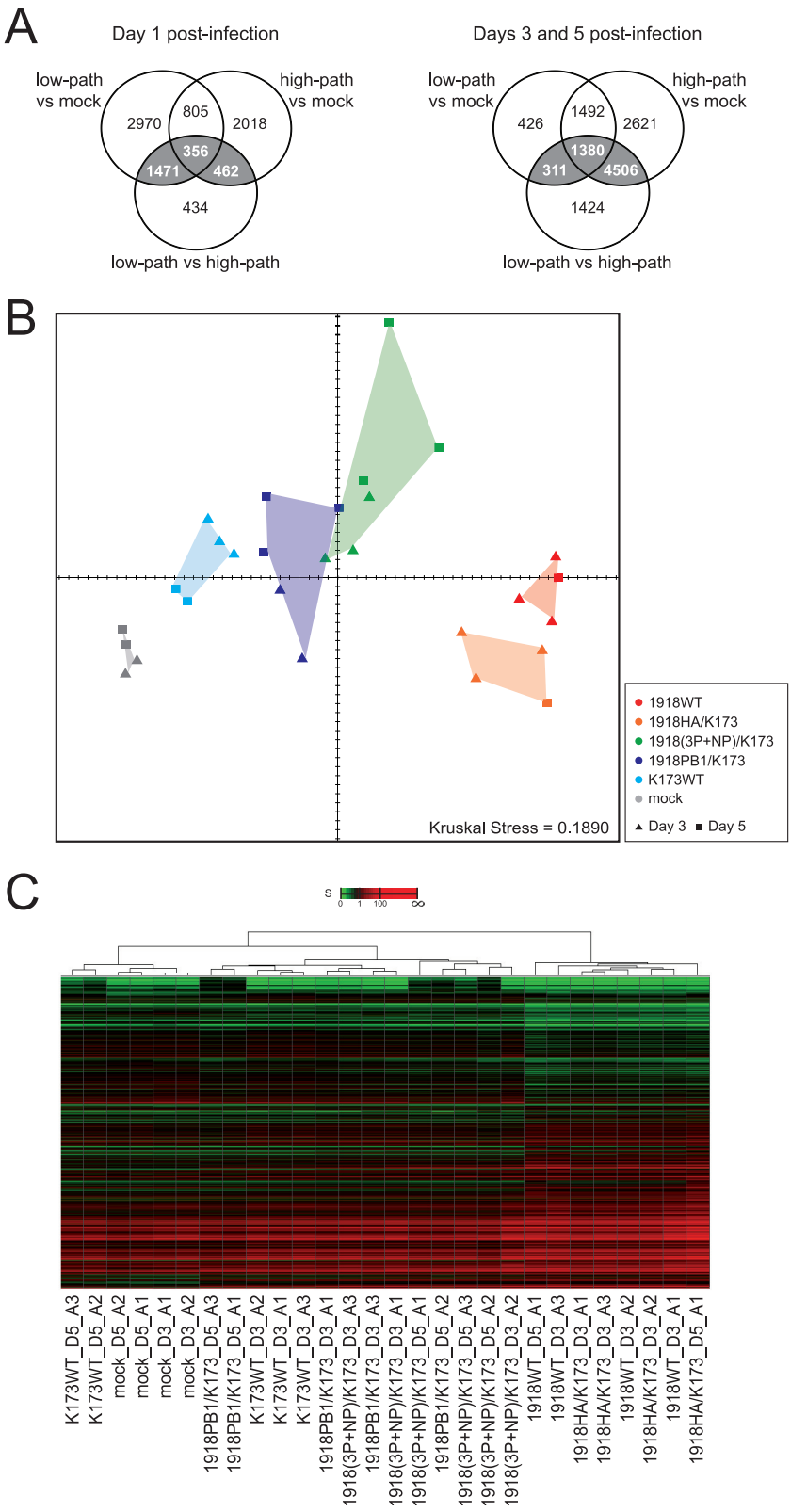

FIG 3 Global analysis of DE genes distinguishing high-pathogenicity and low-pathogenicity virus groups from mock infections. (A) Venn diagram representing the overlap of DE genes in a direct comparison between high-pathogenicity, low-pathogenicity, and mock infections at early (day 1 p.i.) and late (days 3 and 5 p.i.) time points. (B) SVD-MDS representation of the samples on correspondence space with the gene signature applied (6,197 DE genes differentiating low-pathogenicity and high-pathogenicity virus groups from mock infection in at least one group). Each data point represents the RNA expression profile of a single mouse. The convex hull for each set of biological replicates per virus group is shown. The quality of the representation is provided by the Kruskal stress criteria. The *x* and *y* axes represent the relative distance in correspondence space and therefore are unit-free. They correspond to the two first-principle dimensions of the singular value decomposition analysis, which is also the underlying mathematical operation in principle component analysis (PCA). (C) Hierarchical clustering of the signature gene intensities using correspondence metrics. D, day; A, animal; S, signal intensity data.

TABLE 2 Cellular pathways differentially regulated by wild-type and reassortant viruses on day 1 p.i.[a]

Canonical pathway	B-H *P* value[b]	Molecular ratio[c]
Low-pathogenicity-virus vs high-pathogenicity-virus vs mock infection (2,289 DE genes)		
Role of pattern recognition receptors in recognition of bacteria and viruses	2.88E−8	27/106
Interferon signaling	2.40E−6	14/36
Atherosclerosis signaling	8.51E−6	26/136
Communication between innate and adaptive immune cells	8.51E−6	22/109
Cross talk between dendritic cells and natural killer cells	2.09E−5	21/95
1918 virus vs mock infection (3,689 DE genes)		
Dendritic cell maturation	1.00E−16	71/207
Type I diabetes mellitus signaling	6.31E−16	52/120
Communication between innate and adaptive immune cells	1.26E−14	45/109
Role of pattern recognition receptors in recognition of bacteria and viruses	2.00E−14	46/106
Altered T cell and B cell signaling in rheumatoid arthritis	2.51E−14	43/92
1918HA/K173 vs mock infection (4,911 DE genes)		
Communication between innate and adaptive immune cells	2.51E−10	45/109
Altered T cell and B cell signaling in rheumatoid arthritis	2.51E−10	43/92
Dendritic cell maturation	3.98E−10	68/207
Atherosclerosis signaling	2.51E−9	51/136
Role of pattern recognition receptors in recognition of bacteria and viruses	1.00E−8	43/106
1918(3P+NP)/K173 vs mock infection (3,175 DE genes)		
Altered T cell and B cell signaling in rheumatoid arthritis	5.01E−12	36/92
Communication between innate and adaptive immune cells	5.01E−12	37/109
Dendritic cell maturation	6.31E−12	54/207
Role of pattern recognition receptors in recognition of bacteria and viruses	1.58E−8	33/106
Graft-vs-host disease signaling	6.31E−8	21/50

[a] Functional analysis was performed using IPA software.
[b] The Benjamini-Hochberg (B-H) multiple testing correction for *P* values was applied to rank the significance associated for each pathway. Canonical pathway enrichment scores were not statistically significantly different for the 1918PB1/K173-versus-mock infection, K173-versus-mock infection, and 1918 virus-versus-1918HA/K173 comparisons.
[c] Number of molecules differentially expressed within an IPA pathway/total number of molecules within the annotated IPA pathway.

Viral antigen in necrotic cellular debris was observed in the lungs infected with 1918HA/K173 virus (Fig. 2C). In accordance with previous studies (8, 10–12), as 1918HA/K173 virus caused severe lung infection similar to that seen with 1918 virus infection, these results indicate that 1918 virus HA is the primary determinant of enhanced pathogenicity in the 1918 virus infection.

Global analysis of host responses in the lungs of mice infected with wild-type and reassortant viruses. We previously demonstrated that 1918 virus infection in mice leads to enhanced transcriptional activation of innate immune genes related to death receptor, interleukin-6 (IL-6), type I interferon, and Toll-like receptor responses (26). The high replicative ability of 1918HA/K173, 1918PB1/K173, and 1918(3P+NP)/K173 viruses at the early time point indicated that HA and possibly the RNA polymerase and NP of 1918 virus may contribute to aberrant host responses observed with 1918 virus infection in mice. To address this, we profiled transcriptional changes in infected and control mouse lungs at days 1, 3, and 5 p.i. by microarray analysis and examined differentially expressed (DE) genes at early (day 1 p.i.) and late (days 3 and 5 p.i.) phases of acute infection.

A total of 2,289 DE genes and 6,197 DE genes (CDS FC≥ 1.2; $P < 0.01$) distinguished the highly pathogenic viruses (i.e., 1918 and 1918HA/K173; high-pathogenicity virus group) from low-pathogenicity viruses (i.e., K173, 1918PB1/K173, and 1918(3P+NP)/K173; low-pathogenicity virus group), compared to mock infection, in at least one virus group during early (day 1 p.i.) and late (days 3 and 5 p.i.) infection stages, respectively (Fig. 3A, shaded regions). Within the gene sets that distinguished 1918, 1918HA/K173, and 1918(3P+NP)/K173 viruses from mock infection at the early time point, a large proportion of the genes were associated with the canonical pathways known as "communication between innate and adaptive immune cells" and "role of pattern recognition receptors in recognition of bacteria and viruses" (Table 2). Enrichment of these pathways was also observed for 1918(3P+NP)/K173, as well as for the low-pathogenicity 1918PB1/K173 and K173 viruses, at the later time points, whereas the host response to the 1918 and 1918HA/K173 viruses shifted to encompass genes that were primarily associated with the protein ubiquitination pathway (Table 3).

Examination of the 6,197 DE genes that distinguish the high-pathogenicity virus group from the low-pathogenicity virus group compared with mock infection during the late infection stage by use of a multidimensional scaling method initialized by singular value decomposition (SVD-MDS)—a geometric representation of the data set that illustrates similarities and dissimilarities among samples in two-dimensional space—showed a sample distribution at the later time points that correlated with virus pathogenicity (Fig. 3B). There was an apparent divergence of high-pathogenicity and low-pathogenicity virus groups, with greater within-group similarity observed for 1918 and 1918HA/K173 viruses. The SVD-MDS analysis also illustrated a large degree of separation between the high-pathogenicity virus group and the mock infections, indicating that the greatest transcriptional shift in these genes occurred in response to lethal infection, whereas the nonle-

TABLE 3 Cellular pathways differentially regulated by wild-type and reassortant viruses on days 3 and 5 p.i.[a]

Canonical pathway	B-H *P* value[b]	Molecular ratio[c]
Low-pathogenicity-virus vs high-pathogenicity-virus vs mock infection (6,197 DE genes)		
Protein ubiquitination pathway	4.68E−6	101/268
ERK5 signaling	2.00E−3	31/65
Role of macrophages, fibroblasts, and endothelial cells in rheumatoid arthritis	2.00E−3	104/332
Caveolar-mediated endocytosis signaling	2.95E−3	34/85
Acute phase response signaling	3.47E−3	63/178
1918 virus vs mock infection (9,247 DE genes)		
Protein ubiquitination pathway	3.80E−7	134/268
Acute phase response signaling	1.23E−4	88/178
Role of PKR in interferon induction and antiviral response	1.23E−4	29/46
Role of pattern recognition receptors in recognition of bacteria and viruses	1.23E−4	56/106
Hepatic fibrosis/hepatic stellate cell activation	2.63E−4	74/146
1918HA/K173 vs mock (8,902 DE genes)		
Protein ubiquitination pathway	6.03E−10	137/268
Hepatic fibrosis/hepatic stellate cell activation	4.68E−6	77/146
Remodeling of epithelial adherens junctions	1.12E−4	42/68
Apoptosis signaling	2.69E−4	50/95
Role of PKR in interferon induction and antiviral response	5.13E−4	27/46
1918(3P+NP)/K173 vs mock infection (4,692 DE genes)		
Role of pattern recognition receptors in recognition of bacteria and viruses	2.34E−9	46/106
Dendritic cell maturation	9.12E−8	65/207
Type I diabetes mellitus signaling	3.98E−7	45/120
Communication between innate and adaptive immune cells	4.90E−6	39/109
Hepatic fibrosis/hepatic stellate cell activation	1.02E−5	50/146
1918PB1/K173 vs mock infection (2,611 DE genes)		
Role of pattern recognition receptors in recognition of bacteria and viruses	6.03E−9	34/106
Communication between innate and adaptive immune cells	7.41E−8	31/109
LXR/RXR activation	1.41E−7	36/136
Cross talk between dendritic cells and natural killer cells	4.47E−7	29/95
Hepatic fibrosis/hepatic stellate cell activation	1.41E−6	37/146
K173 vs mock infection (2,913 DE genes)		
Cell cycle control of chromosomal replication	7.24E−9	18/31
Role of pattern recognition receptors in recognition of bacteria and viruses	2.40E−8	35/106
Cross talk between dendritic cells and natural killer cells	6.76E−7	31/95
Antigen presentation	2.19E−6	18/40
Communication between innate and adaptive immune cells	1.20E−5	29/109
1918 virus vs 1918HA/K173 infection (283 DE genes)		
Interferon signaling	3.47E−3	5/36
Role of JAK1, JAK2, and TYK2 in interferon signaling	7.41E−3	4/27
IL-15 production	7.94E−3	4/31
Retinoic acid-mediated apoptosis signaling	1.86E−2	5/69
Cross talk between dendritic cells and natural killer cells	6.46E−2	5/95

[a] Differentially expressed genes were identified using the CDS statistical test (FC $\geq$ 1.2; $P < 0.01$).
[b] Functional analysis was performed using IPA software. Benjamini-Hochberg (B-H) multiple testing correction for the *P* value was applied to rank the significance associated for each pathway.
[c] Number of molecules differentially expressed within an IPA pathway/total number of molecules within the annotated IPA pathway.

thal viruses resulted in a less pronounced transcriptional response phenotype (Fig. 3B). Hierarchical clustering of the expression of these genes confirmed similarity of 1918 and 1918HA/K173 viruses based on the sample groupings and greater magnitude of response to the lethal viruses than to the nonlethal viruses (Fig. 3C). Taken together, these results suggest that HA of 1918 virus induces a transcriptional signature comparable to that of the fully reconstructed 1918 virus that is not observed with K173 recombinant viruses expressing either 1918 PB1 alone or 1918 RNA polymerase and NP.

1918 and 1918HA/K173 viruses evoke similar, though not identical, host responses. Previous studies have shown increased activation of proinflammatory, pronecrotic, and stress response genes in the lung in response to recombinant viruses expressing 1918 NA and HA genes, viral determinants associated with high pathogenicity (25, 26). Here, we show that K173 recombinant

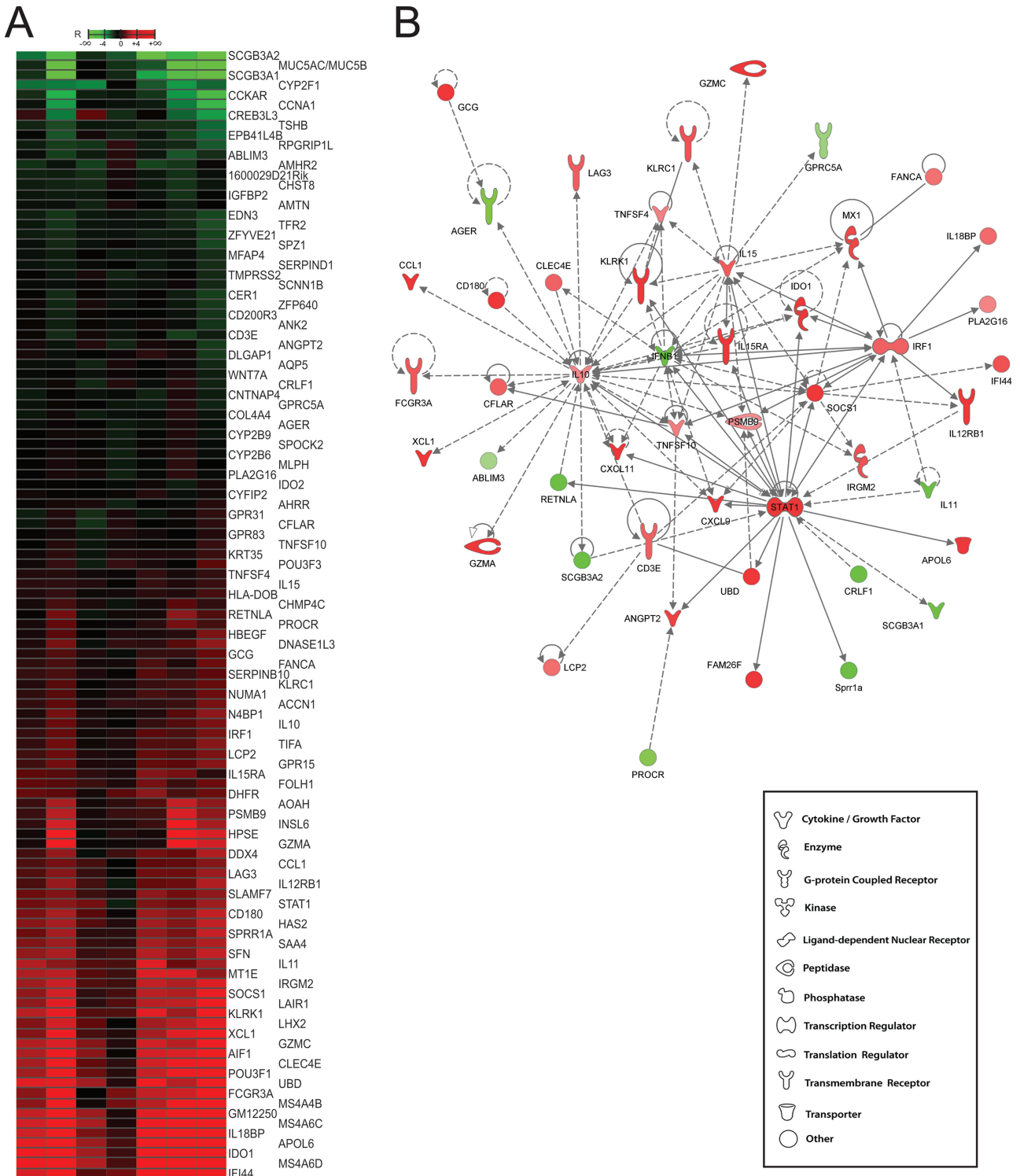
A
R
-∞ -4 0 +4 +∞
SCGB3A2
SCGB3A1
CCKAR
CREB3L3
EPB41L4B
ABLIM3
1600029D21Rik
IGFBP2
EDN3
ZFYVE21
MFAP4
TMPRSS2
CER1
CD200R3
CD3E
DLGAP1
WNT7A
CNTNAP4
COL4A4
CYP2B9
CYP2B6
PLA2G16
CYFIP2
GPR31
GPR83
KRT35
TNFSF4
HLA-DOB
RETNLA
HBEGF
GCG
SERPINB10
NUMA1
N4BP1
IRF1
LCP2
IL15RA
DHFR
PSMB9
HPSE
DDX4
LAG3
SLAMF7
CD180
SPRR1A
SFN
MT1E
SOCS1
KLRK1
XCL1
AIF1
POU3F1
FCGR3A
GM12250
IL18BP
IDO1
IFI44
MX1
CXCL9
MUC5AC/MUC5B
CYP2F1
CCNA1
TSHB
RPGRIP1L
AMHR2
CHST8
AMTN
TFR2
SPZ1
SERPIND1
SCNN1B
ZFP640
ANK2
ANGPT2
AQP5
CRLF1
GPRC5A
AGER
SPOCK2
MLPH
IDO2
AHRR
CFLAR
TNFSF10
POU3F3
IL15
CHMP4C
PROCR
DNASE1L3
FANCA
KLRC1
ACCN1
IL10
TIFA
GPR15
FOLH1
AOAH
INSL6
GZMA
CCL1
IL12RB1
STAT1
HAS2
SAA4
IL11
IRGM2
LAIR1
LHX2
GZMC
CLEC4E
UBD
MS4A4B
MS4A6C
APOL6
MS4A6D
FAM26F
IFNB1
CXCL11
LPV
HPV
K173 WT
1918PB1/K173
1918(3P+NP)/K173
1918HA/K173
1918 WT
B
GCG
GZMC
LAG3
KLRC1
GPRC5A
FANCA
AGER
TNFSF4
MX1
IL18BP
IL15
CCL1
CLEC4E
KLRK1
CD180
IDO1
PLA2G16
IL15RA
IRF1
IFNB1
IL10
IFI44
FCGR3A
CFLAR
SOCS1
PSMB9
IL12RB1
XCL1
TNFSF10
CXCL11
ABLIM3
IRGM2
RETNLA
STAT1
IL11
CXCL9
GZMA
APOL6
SCGB3A2
CD3E
UBD
CRLF1
ANGPT2
SCGB3A1
LCP2
FAM26F
Sprr1a
PROCR
Cytokine / Growth Factor
Enzyme
G-protein Coupled Receptor
Kinase
Ligand-dependent Nuclear Receptor
Peptidase
Phosphatase
Transcription Regulator
Translation Regulator
Transmembrane Receptor
Transporter
Other

virus expressing 1918 virus HA alone induces a pronounced transcriptional response similar to that induced by 1918 virus in mice. Functional analysis of DE genes from 1918HA/K173-infected mouse lung revealed significant enrichment of genes associated with the protein ubiquitination pathway as well as the canonical pathways "hepatic fibrosis/hepatic stellate cell activation," "remodeling of epithelial adherens junctions," "apoptosis signaling," and "role of PKR in interferon induction and antiviral response" (Table 3). Significant enrichment of genes associated with the protein ubiquitination pathway and the canonical pathway "hepatic fibrosis/hepatic stellate cell activation" also characterized 1918 virus infection, indicating that 1918 and 1918HA/K173 viruses may impact similar cellular pathways contributing to the same pathological outcome.

Despite similarities in the clinical course of and global host response to infection, a total of 283 genes distinguished 1918 virus from 1918HA/K173 virus, and within this set of genes, there was representation of genes associated with the canonical pathways "interferon signaling," "IL-15 production," "retinoic acid-mediated apoptosis signaling," and "cross talk between dendritic cells and natural killer cells." Highly upregulated chemokine CXCL9 and CXCL11 genes and the proapoptotic APOL6 gene were induced more than 2-fold in response to 1918 virus compared with 1918HA/K173 virus (Fig. 4; Table 4). Secretoglobin (SCGB) superfamily SCGB3A1 and SCGB3A2 genes were strongly downregulated in response to both high-pathogenicity viruses and even more strongly downregulated in response to 1918 virus than in response to 1918HA/K173 virus. Interestingly, there was marked expression of IFNB1 in response to 1918HA/K173, which was induced more than 2-fold relative to 1918 virus (Fig. 4; Table 4). Differential induction of genes related to T lymphocyte cytotoxicity and NK cell proliferation was also observed. In infected lungs, compared to 1918HA/K173 virus, 1918 virus elicited greater upregulation of IL-15, IL15RA, KLRK1 (also known as NKG2D), and KLRC1 genes, which are known to regulate maturation of NK cells in lung immunopathology during influenza infection (Fig. 4; Table 4) (27). These data suggest that exacerbated NK cell activity at later time points in the acute phase may contribute to 1918 and 1918HA/K173 pathogenesis in mice, and the difference in magnitude of gene expression may account for the accelerated morbidity and mortality following 1918 infection compared to 1918HA/K173 infection.

The highly pathogenic viruses induced the transcriptional activity of proinflammatory genes during the acute phase. Analysis of DE genes related to acute-phase responses revealed that 1918 and 1918HA/K173 viruses strongly upregulated IL-6 gene expression that was approximately 10-fold higher in the high-pathogenicity virus group than in the low-pathogenicity virus group (Table 5), concomitant with elevated IL-6 cytokine levels in mouse lungs infected with either 1918 virus (28) or a recombinant virus expressing 1918 virus HA (10). We observed an increase in IL-6 signaling pathway genes, including increased expression of the transcription factor genes STAT3 and NF-IL-6, the heme-related target protein genes HPX and HMOX1, and the complement component genes C1R and C2 (Fig. 5A and Table 5).

Infection with 1918 or 1918HA/K173 virus results in polymorphonuclear cell infiltration into mouse lungs, and we therefore investigated molecular signaling events likely promoting leukocyte recruitment. Inflammatory response genes affiliated with leukocyte immune cell functions, such as cell activation, accumulation, and movement, were upregulated in 1918- and 1918HA/K173-infected lungs compared to K173- and 1918PB1/K173-infected lungs, though many of these genes were also observed to be upregulated to a similar extent in the lungs during 1918(3P+NP)/K173 virus infection as in the high-pathogenicity virus group (Fig. 5B).

Overall, these data suggest that, relative to less pathogenic viruses, the highly pathogenic viruses enhance proinflammatory transcriptional responses in mice, such as enhanced IL-6 expression, upregulation of IL-6 signaling pathway genes, enhanced leukocyte responses, and, in particular, enhanced neutrophil activity.

1918(3P+NP)/K173 and high-pathogenicity viruses differentially regulate genes related to the immunoproteasome-MHC class I presentation pathway. Protein ubiquitination pathway genes were commonly differentially expressed by 1918 and 1918HA/K173 viruses at late time points of the acute phase (Table 3). We examined functional relationships for 56 genes changing more than 2-fold in both 1918 and 1918HA/K173 infections (Fig. 6A). There was representation of genes related to protein ubiquitination (UBE2L6 and UBE4A), catabolism of ATP (PSMC1, PSMC5, and PSMC6), protein folding (B2M and HSPB1), and the degradation of ubiquitin-protein conjugates (USP18 and USP3). Interestingly, we observed that genes associated with the immunoproteasome and antigen presentation were strongly expressed by 1918(3P+NP)/K173 virus (FC $\geq$ 2) relative to K173 virus, including IFNG, immunoproteasome subunits, PSMB8, PSMB9, and PSMB10, antigen transporter, TAP1 and TAP2, UBD, and the ISG15-specific protease USP18 (Table 6). Gamma interferon (IFN-γ) stimulates immunoproteasomes (29), which function in production of peptides derived from endogenous proteins that are translocated by IFN-γ-induced TAP1 and TAP2 into the endoplasmic reticulum, where they bind to major histocompatibility complex (MHC) class I molecules for transport to the cell surface, promoting the antigen presentation to cytotoxic T lymphocytes (CTLs) (reviewed in reference 30). Among those genes, IFNG, PSMB9, and USP18 were more highly expressed in response to 1918(3P+NP)/K173 virus than in response to the high-pathogenicity virus group (Table 6).

We further investigated genes whose expression was increased in the high-pathogenicity virus group compared to 1918(3P+NP)/K173 virus. Genes encoding heat shock proteins (e.g., HSPA9,

FIG 4 1918 and 1918HA/K173 viruses differentially regulate lymphocyte gene expression in lungs of the virus-infected mice. (A) The heatmap shows a total of 118 DE genes that were available for analysis in IPA. Average $\log_2$(ratio) gene expression in infected lungs relative to that in mock-infected lungs is shown. Saturation is 3-fold. Red indicates that the gene expression is higher than that in the uninfected reference; green indicates that gene expression is lower than that in the uninfected reference. LPV, low-pathogenicity virus group; HPV, high-pathogenicity virus group. (B) Pathway analysis diagram showing the functional relationships among DE genes differentially regulated between 1918 and 1918HA/K173 viruses. Average lung gene expression for 1918 virus relative to 1918HA/K173 virus is overlaid onto the network. Nodes shaded red indicates that 1918 virus-induced gene expression is higher than the gene expression induced by the 1918HA/K173 reference; green indicates that 1918 virus-induced gene expression is lower than that induced by the 1918HA/K173 reference. R, log ratio data.

TABLE 4 Differentially expressed genes distinguishing 1918 and 1918HA/K173 viruses on days 3 and 5 p.i.[a]

Gene symbol	Entrez gene name	Gene ID	Change (fold) in expression induced by[b]: 1918 virus	1918HA/K173
ABLIM3	Actin binding LIM protein family, member 3	NM_198649	−2.20	−1.56
AGER	Advanced glycosylation end product-specific receptor	NM_007425	−1.18	1.46
ANGPT2	Angiopoietin 2	NM_007426	−1.04	−1.75
APOL6	**Apolipoprotein L, 6**	**AK010208**	**35.49**	**17.15**
CCL1	**Chemokine (C-C motif) ligand 1**	**NM_011329**	**6.86**	**3.40**
CD180	CD180 molecule	NM_008533	8.32	4.36
CD3E	CD3e molecule, epsilon (CD3-TCR complex)	BC028636	−1.13	−1.73
CFLAR	CASP8 and FADD-like apoptosis regulator	Y14041	1.73	1.13
CLEC4E	C-type lectin domain family 4, member E	NM_019948	17.27	11.28
CRLF1	Cytokine receptor-like factor 1	NM_018827	−1.42	1.51
CXCL11	**Chemokine (C-X-C motif) ligand 11**	**NM_019494**	**878.00**	**341.07**
CXCL9	**Chemokine (C-X-C motif) ligand 9**	**NM_008599**	**283.10**	**117.36**
FAM26F	**Family with sequence similarity 26, member F**	**NM_175449**	**50.71**	**21.00**
FANCA	Fanconi anemia, complementation group A	NM_016925	2.85	1.95
FCGR3A	Fc fragment of IgG, low affinity IIIa, receptor (CD16a)	NM_144559	22.18	14.04
GCG	**Glucagon**	**NM_008100**	**3.90**	**1.60**
GPRC5A	G protein-coupled receptor, family C, group 5, member A	NM_181444	−1.09	1.34
GZMA	Granzyme A (granzyme 1, cytotoxic T-lymphocyte-associated serine esterase 3)	NM_010370	5.95	3.29
GZMC	**Granzyme C**	**NM_010371**	**19.69**	**5.61**
IDO1	**Indoleamine 2,3-dioxygenase 1**	**NM_008324**	**39.62**	**19.36**
IFI44	Interferon-induced protein 44	AK085407	37.82	23.55
IFNB1	Interferon, beta 1, fibroblast	NM_010510	61.24	131.86
IL-10	Interleukin 10	NM_010548	3.32	2.40
IL-11	Interleukin 11	NM_008350	10.36	24.89
IL12RB1	**Interleukin 12 receptor, beta 1**	**NM_008353**	**8.52**	**3.87**
IL-15	Interleukin 15	NM_008357	2.31	1.48
IL15RA	Interleukin 15 receptor, alpha	NM_008358	4.71	2.70
IL18BP	Interleukin 18 binding protein	NM_010531	30.33	20.30
IRF1	Interferon regulatory factor 1	NM_008390	3.80	2.48
IRGM2	Immunity-related GTPase family M member 2	NM_019440	10.93	6.82
KLRC1	Killer cell lectin-like receptor subfamily C, member 1	NM_010652	3.30	2.06
KLRK1	Killer cell lectin-like receptor subfamily K, member 1	NM_033078	14.02	7.44
LAG3	Lymphocyte activation gene 3	NM_008479	6.94	4.47
LCP2	Lymphocyte cytosolic protein 2 (SH2 domain containing leukocyte protein of 76 kDa)	NM_010696	3.91	2.66
MX1	Myxovirus (influenza virus) resistance 1, interferon-inducible protein p78 (mouse)	NM_010846	67.64	40.55
PLA2G16	Phospholipase A2, group XVI	AK052657	1.03	−1.35
PROCR	Protein C receptor, endothelial	NM_011171	2.24	3.72
PSMB9	Proteasome (prosome, macropain) subunit, beta type, 9 (large multifunctional peptidase 2)	NM_013585	4.76	3.50
RETNLAa	Resistin like alpha	NM_020509	1.65	3.72
SCGB3A1	Secretoglobin, family 3A, member 1	NM_170727	−18.26	−9.30
SCGB3A2	**Secretoglobin, family 3A, member 2**	**NM_054038**	**−35.21**	**−16.34**
SOCS1	Suppressor of cytokine signaling 1	NM_009896	12.73	6.87
SPRR1A	Small proline-rich protein 1A	NM_009264	4.77	10.16
STAT1	Signal transducer and activator of transcription 1, 91 kDa	AK041599	8.29	4.38
TNFSF10	Tumor necrosis factor (ligand) superfamily, member 10	NM_009425	1.84	1.30
TNFSF4	Tumor necrosis factor (ligand) superfamily, member 4	NM_009452	2.06	1.46
UBD	**Ubiquitin D**	**NM_023137**	**26.22**	**12.30**
XCL1	**Chemokine (C motif) ligand 1**	**NM_008510**	**17.45**	**7.44**

[a] Differentially expressed genes (FC ≥ 1.2) between 1918 and 1918HA/K173 viruses, as shown in Fig. 4B.
[b] Relative to expression in mock-infected lungs. Bold type signifies changes in gene expression induced by 1918 virus (FC ≥ 2) relative to 1918HA/K173.

HSPB1, HSPB7, and HSPB8), catalytic and regulatory proteasome subunits (e.g., PSMC1, PSMD12, PSMD13, PSMD14, PSMD4, and PSMD8), and ubiquitin-specific peptidases (e.g., UBE2D3, UBE2J1, UBE2J2, and UCHL5) were more highly expressed by the high-pathogenicity virus group (FC ≥ 1.5) than by 1918/K173 virus (Table 6). Intriguingly, the UBE4A gene, encoding ubiquitin conjugation factor E4 A, which functions in multiubiquitin chain assembly, was upregulated by the high-pathogenicity virus group, whereas it was downregulated by the low-pathogenicity virus group.

These data indicate that high viral replication early in infection is associated with the subsequent increased expression of genes within the immunoproteasome-MHC class I presentation pathway during the acute phase.

TABLE 5 Differential expression of acute-phase response signaling genes during low- and high-pathogenicity virus infection on days 3 and 5 p.i.[a]

Gene symbol	Entrez gene name	Gene ID	Change (fold) in expression induced by[b]: LPV	HPV
C1R	Complement component 1, r subcomponent	AF459018	2.41	3.65
C2	**Complement component 2**	**NM_013484**	**2.60**	**5.44**
CP	Ceruloplasmin (ferroxidase)	NM_007752	3.22	6.13
HMOX1	**Heme oxygenase (decycling) 1**	**NM_010442**	**1.29**	**5.90**
HPX	**Hemopexin**	**NM_017371**	**3.23**	**10.95**
IL-6	**Interleukin 6 (interferon, beta 2)**	**NM_031168**	**18.64**	**181.90**
ITIH4	Inter-alpha (globulin) inhibitor H4 (plasma Kallikrein-sensitive glycoprotein)	NM_018746	1.54	−1.47
JAK2	Janus kinase 2	NM_008413	1.46	2.57
NF-IL-6	CCAAT/enhancer binding protein (C/EBP), beta	NM_009883	1.62	2.96
OSM	Oncostatin M	NM_001013365	2.53	4.05
OSMR	**Oncostatin M receptor**	**NM_011019**	**1.38**	**3.83**
ORM1/2	**Orosomucoid 1**	**NM_008768**	**5.42**	**15.44**
SAA1	**Serum amyloid A1**	**NM_011315**	**55.76**	**202.78**
SERPINA1	Serpin peptidase inhibitor, clade A (alpha-1 antiproteinase, antitrypsin), member 1	BC037008	1.47	1.95
SERPINA3	**Serpin peptidase inhibitor, clade A (alpha-1 antiproteinase, antitrypsin), member 3**	**NM_009252**	**4.15**	**43.13**
SERPING1	Serpin peptidase inhibitor, clade G (C1 inhibitor), member 1	NM_009776	2.04	3.45
SHP2	**Protein tyrosine phosphatase, non-receptor type 11**	**NM_011202**	**−1.20**	**1.80**
SOCS1	**Suppressor of cytokine signaling 1**	**NM_009896**	**4.77**	**9.80**
SOCS3	**Suppressor of cytokine signaling 3**	**NM_007707**	**2.25**	**9.30**
SOD2	**Superoxide dismutase 2, mitochondrial**	**NM_013671**	**1.58**	**3.96**
STAT3	**Signal transducer and activator of transcription 3 (acute-phase response factor)**	**ENSMUST00000103114**	**−1.33**	**2.41**

[a] Differentially expressed acute phase response signaling genes (FC ≥ 1.2) for low-pathogenicity virus (LPV) and high-pathogenicity virus (HPV) groups, as shown in Fig. 5A.
[b] Relative to expression in mock-infected lungs. Bold type signifies changes in gene expression induced by HPV (FC ≥ 2) relative to LPV.

DISCUSSION

Previous studies have shown that HA contributes to efficient replication and high virulence of the 1918 virus in a mouse model (8, 10–12), although it remains unclear whether the high replication ability or the 1918 virus HA gene by itself is the more important element for 1918 virus to exhibit high virulence in mice. To evaluate this, we systematically studied reassortant viruses derived from the 1918 virus and a contemporary human H1N1 virus (A/Kawasaki/173/2001 [K173]). Here we show that the K173 recombinant virus possessing 1918 polymerase complex genes, i.e., the PA, PB1, PB2, and NP genes [i.e., 1918(3P+NP)/K173 virus], replicated efficiently early in infection and to the same extent as the 1918 virus in mouse lungs, although infected mice were asymptomatic, whereas a virus possessing the 1918 virus HA gene exhibited efficient replication and high virulence in mice. Moreover, we demonstrated that the K173(3P+NP)/1918 virus, possessing HA, NA, M, and NS genes from 1918 virus and the remaining genes from K173 virus, was lethal to mice when the mice were infected with a high dose of virus, despite its inefficient virus growth in mouse lungs (Table 1). Thus, our results suggest that not only the capacity for a high level of replication but also the 1918 virus HA gene itself are required for high pathogenicity in mice.

In general, viral infection induces innate immune and adaptive immune responses. A recent comprehensive genomic analysis detailed host responses to influenza virus over a 60-day period that encompassed acute, intermediate, and late stages of infection (31). This study showed expression changes in cell-specific gene signatures over the infection course, such as NK cell gene expression during the acute phase that peaked at day 5 p.i. and T cell gene expression that was initiated at day 5 p.i. and continued into the intermediate and late stages of infection. In most cases, the initial viral replication is controlled by innate immune responses at the early time of infection, and virus is subsequently cleared from the host. The 1918(3P+NP)/K173 virus replicated to the same extent as the 1918 virus in mouse lungs early in infection; however, viral replication might be controlled by innate immune responses, resulting in a decrease in virus titers at days 3 and 5 p.i. Differential induction of genes related to communication between innate and adaptive immune cells, such as NK cells, implied that the suppression of acute-phase responses and the transition to adaptive immunity had occurred in low-pathogenicity-virus infection. In contrast, the host failed to control the initial replication of the high-pathogenicity virus possessing the 1918 virus HA gene, resulting in a sustained high viral load that overextended inflammatory responses during acute infection (Fig. 1, 2, and 5), despite strong expression of genes related to negative feedback regulators of proinflammatory responses (e.g., suppressors of cytokine signaling [SOCS1 and SOCS3]) (Table 5). Inflammatory mediators of acute infection, such as tumor necrosis factor (TNF), IL-1-α/β, and IL-6, can appreciably influence influenza virus-associated pathology. For example, mice infected with 1918 virus showed increased survival in the absence of TNF receptor (TNFR) signaling, indicating that TNF exerts potent activity during 1918 virus infection (32). Thus, hyperinduction and persistent expression of inflammatory response genes by the high-pathogenicity virus group may provoke an immune response that leads to immunopathology rather than repairing processes in mouse lungs.

Characterization of 1918 virus genetic markers of high virulence is important for understanding viral determinants contributing to pandemic strains with high pathogenicity. Previous genomic analysis of mouse lungs infected with recombinant

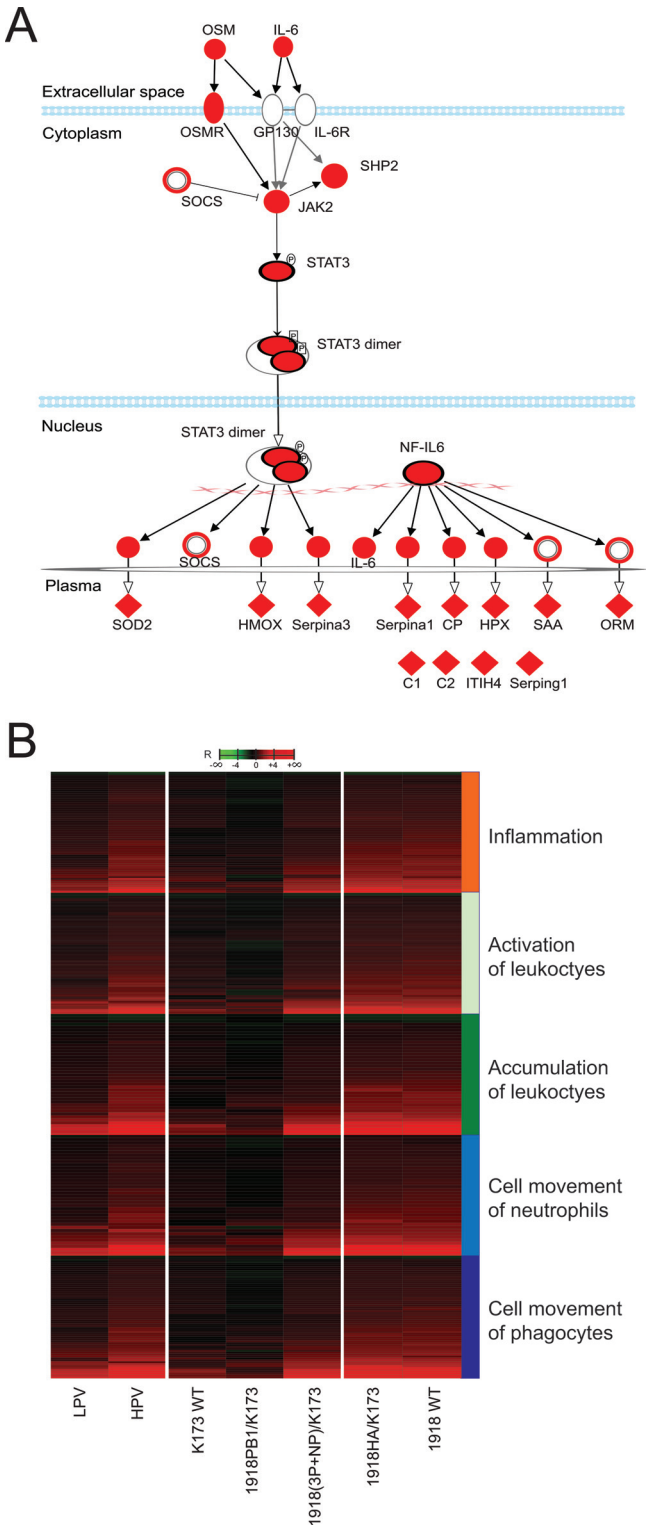

FIG 5 Mice show differential expression of genes associated with acute-phase responses during infection. (A) Differentially expressed IL-6 signaling pathway molecules. Molecules shaded in red were differentially upregulated between low-pathogenicity and high-pathogenicity virus groups. Red indicates upregulation relative to mock infection. Open circles signify group complexes. Transcriptional target genes encoding plasma molecules are indicated with diamonds. Genes depicting cellular pathway molecules or transcriptional target genes are depicted by circles. (B) Transcriptional changes of 134 inflammatory response genes in response to infection. Average $\log_2$(ratio) gene expression of infected lung relative to mock is shown. Saturation is 3-fold. Red indicates that the gene expression is higher than that in the uninfected reference; green indicates that gene expression is lower than that in the uninfected reference. LPV, low-pathogenicity virus group; HPV, high-pathogenicity virus group; R, log ratio data.

viruses expressing the HA and NA genes of the 1918 virus in the genetic background of either mouse-adapted influenza A/WSN/33 virus (1918HA/NA:WSN) or Tx/91 virus (1918HA/NA:Tx/91) showed differential expression of proinflammatory, cell death, and stress response genes (25), although not all 1918 virus genes contribute to virulence. For example, the 1918 virus NS gene in the genetic background of WSN or Tx/91 did not confer a more virulent phenotype (11, 33), though 1918 virus NS1 is reported to have potent IFN antagonist activity (34). We have confirmed these findings by showing that 1918 virus NS in the genetic background of seasonal human influenza K173 virus did not result in increased virulence in mice (Table 1). Further, we show for the first time that the 1918 viral RNA polymerase, though important for high replication efficiency, does not cause lethality in mice, whereas HA alone is sufficient to contribute to 1918 virus virulence by facilitating efficient viral replication and triggering a more severe and sustained inflammatory response.

One hypothesis of how 1918 virus HA might affect the host's innate response network to drive pathogenesis is that it accelerates the network's dynamics rather than affecting the network structure itself. This proposition would provide an explanation of why it is difficult to define the host factors driving pathogenicity during influenza virus infection. A similar proposal has been made recently for simian immunodeficiency virus infection in natural hosts versus progressor species (35). Based on a recent meta-analysis of transcriptome data from respiratory virus infections in mice (36), the hypothesis of dynamic encoding of host responses has been extended to influenza viruses (37).

SVD-MDS analysis and unsupervised hierarchical clustering of the pathogenicity gene signature defined in our study illustrated the divergence in host response to the 1918 and 1918HA/K173 viruses compared to the low-pathogenicity viruses. These analyses indicated that, among these genes, the host transcriptional response was notably more pronounced in the lungs of mice infected with the lethal viruses, including genes associated with ubiquitin-proteasome pathway (Table 6). Among them, IFNG and USP18 genes were most highly expressed in the high-pathogenicity group, and their expression was also strongly induced by 1918(3P+NP)/K173 virus infection. IFN-γ has roles in inhibition of viral replication, stimulation of CTL, increasing MHC I expression, activation of macrophages and neutrophils, and promoting T-cell proliferation (reviewed in references 38 and 39). A previous study suggested that the presence of IFN-γ improves the severity of inflammation and lung damage (40). In accordance with this, the strong induction of IFN-γ may in part result in inhibition of viral replication and also prevent immunopathology in mice infected with 1918(3P+NP)/K173 virus; however, this is not the case with the high-pathogenicity virus group, presumably because of the 1918 virus HA function. The product of the other highly expressed gene, USP18 (ubiquitin-specific peptidase 18), is a member of the deubiquitinating protease family and specifically cleaves ISG15 (interferon-stimulated gene 15) from its protein

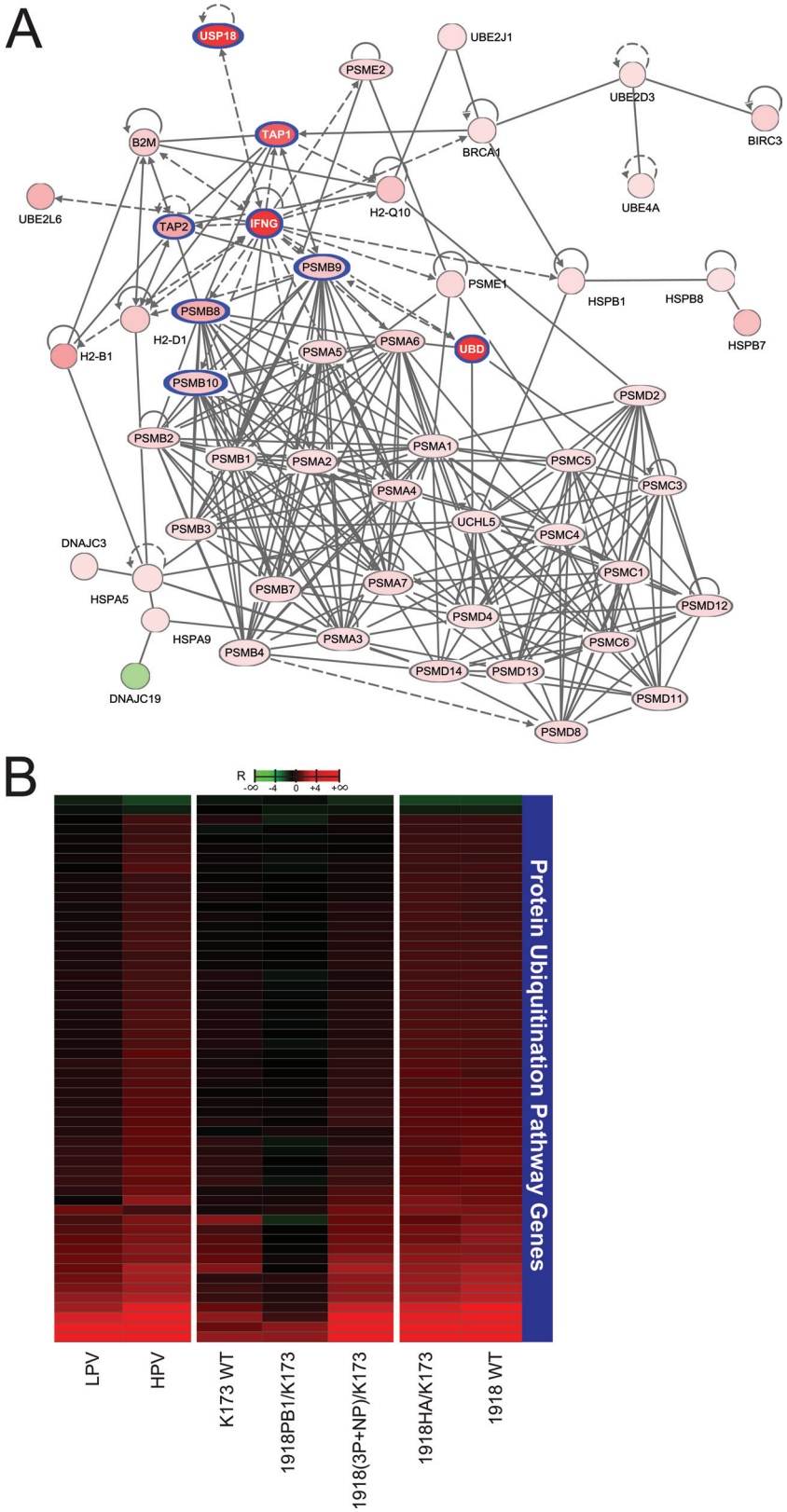

FIG 6 The protein ubiquitination pathway is similarly activated by 1918 and 1918HA/K173. (A) Ingenuity pathway analysis (IPA) of the 56 DE genes. Direct functional relationships between pathway nodes were examined, and orphan molecules were eliminated. The remaining 52 DE genes are shown in the diagram with an overlay of the average $\log_2$(ratio) gene expression of the high-pathogenicity virus group relative to that seen in mock infection. Red signifies upregulation in the high-pathogenicity virus group relative to mock infection, and green signifies downregulation. Genes outlined in blue exhibited increased expression in 1918(3P+NP)/K173-infected lungs relative to K173-infected lungs. (B) Heatmap of average $\log_2$(ratio) gene expression of infected lung relative to mock infection. Saturation is 3-fold. Red indicates that the gene expression is higher than in the mock-infected reference; green indicates that gene expression is lower than in the mock-infected reference. LPV, low-pathogenicity virus group; HPV, high-pathogenicity virus group; R, log ratio data.

TABLE 6 Protein ubiquitination pathway genes differentially regulated during 1918(3P+NP)/K173 and high-pathogenicity-virus infections on days 3 and 5 p.i.[a]

Gene symbol	Gene ID	Change (fold) in expression induced by indicated virus relative to mock infection				Change (fold) in expression induced by 1918(3P+NP)/K173 relative to K173[b]	Change (fold) in expression induced by HPV relative to 1918(3P+NP)/K173[c]
		K173	1918(3P+NP)/K173	LPV	HPV		
B2M	NM_009735	2.20	3.23	2.60	3.73	1.47	1.15
BIRC3	NM_007464	1.45	1.99	1.69	3.45	1.37	1.74
BRCA1	NM_009764	4.39	3.22	3.45	2.17	0.73	0.67
CDC34	NM_177613	1.23	1.34	1.27	2.22	1.08	1.66
DNAJC19	AK076602	−1.23	−1.64	−1.40	−2.10	1.34	1.28
DNAJC3	NM_008929	1.12	1.47	1.27	2.34	1.31	1.59
H2-Q10	NM_010391	2.75	3.67	3.14	4.35	1.34	1.18
H2-B1	NM_008199	4.26	6.21	5.07	7.25	1.46	1.17
H2-D1	NM_010380	2.65	3.47	2.96	3.98	1.31	1.15
HSPA4L	AK050997	−1.58	−1.66	−1.57	−2.02	1.05	1.22
HSPA5	NM_022310	−1.07	1.43	1.22	2.04	1.34	1.42
HSPA9	NM_010481	1.06	1.20	1.11	2.30	1.13	1.91
HSPB1	NM_013560	−1.16	1.17	−1.01	2.55	1.00	2.19
HSPB7	NM_013868	1.12	1.02	1.11	4.77	0.91	4.66
HSPB8	NM_030704	1.15	1.18	1.16	2.34	1.03	1.98
IFNG	NM_008337	5.16	64.54	33.64	33.49	**12.50**	0.52
PSMA1	NM_011965	1.26	1.66	1.39	2.30	1.32	1.39
PSMA2	NM_008944	1.23	1.75	1.46	2.52	1.42	1.44
PSMA3	NM_011184	−1.46	1.69	1.50	2.63	1.15	1.56
PSMA4	NM_011966	1.72	1.76	1.73	2.97	1.02	1.69
PSMA5	NM_011967	1.21	1.93	1.52	2.83	1.60	1.47
PSMA6	NM_011968	1.94	2.09	1.91	3.36	1.08	1.61
PSMA7	NM_011969	1.15	2.08	1.56	3.02	1.81	1.45
PSMB1	NM_011185	1.44	1.53	1.42	2.22	1.06	1.45
PSMB2	NM_011970	1.69	2.10	1.81	3.17	1.24	1.51
PSMB3	NM_011971	1.13	1.56	1.28	2.18	1.38	1.40
PSMB4	NM_008945	1.25	1.67	1.40	2.33	1.34	1.39
PSMB7	NM_011187	1.60	1.82	1.63	2.51	1.14	1.38
PSMB8	NM_010724	2.01	5.16	3.52	6.04	**2.56**	1.17
PSMB9	NM_013585	2.11	4.71	3.37	4.13	**2.24**	0.88
PSMB10	NM_013640	1.27	3.51	2.31	4.00	**2.77**	1.14
PSMC1	NM_008947	1.41	1.36	1.32	2.49	0.96	1.84
PSMC3	NM_008948	1.12	1.54	1.28	2.06	1.38	1.34
PSMC4	NM_011874	1.34	1.53	1.38	2.25	1.14	1.47
PSMC5	NM_008950	1.07	1.87	1.40	2.07	1.75	1.11
PSMC6	NM_025959	1.27	1.53	1.34	2.44	1.21	1.59
PSMD11	NM_178616	−1.36	1.51	1.23	2.15	1.11	1.43
PSMD12	NM_025894	1.14	1.54	1.30	2.87	1.35	1.87
PSMD13	NM_011875	1.38	1.51	1.42	2.72	1.10	1.80
PSMD14	NM_021526	−1.59	1.59	1.44	2.84	1.00	1.79
PSMD2	NM_134101	1.29	1.51	1.36	2.16	1.17	1.43
PSMD4	NM_008951	1.19	1.42	1.27	2.28	1.20	1.60
PSMD8	NM_026545	1.75	1.53	1.56	2.75	0.87	1.80
PSME1	NM_011189	1.29	2.56	1.85	2.89	1.99	1.13
PSME2	NM_011190	1.37	2.68	1.98	3.12	1.96	1.16
TAP1	NM_013683	3.20	9.06	6.07	12.29	**2.83**	1.36
TAP2	NM_011530	1.67	4.81	3.19	6.60	**2.89**	1.37
UBD	NM_023137	3.32	34.90	18.98	19.26	**10.50**	0.55
UBE2D3	NM_025356	−1.24	1.22	1.13	2.10	0.98	1.73
UBE2J1	NM_019586	1.12	1.50	1.26	2.54	1.33	1.70
UBE2J2	NM_021402	−1.40	1.32	1.32	2.45	0.94	1.85
UBE2L6	NM_019949	3.14	4.86	3.98	5.74	1.55	1.18
UBE4A	NM_145400	−1.17	−1.14	−1.13	2.21	0.97	1.94
UCHL5	NM_019562	1.15	1.18	1.12	2.08	1.03	1.76
USP3	NM_144937	1.47	1.21	10.33	2.01	0.82	1.66
USP18	NM_011909	4.87	14.82	1.24	21.48	**3.04**	1.45

[a] Differentially expressed protein ubiquitination genes (FC ≥ 1.2) for K173, 1918(3P+NP)/K173, low-pathogenicity virus (LPV), and high-pathogenicity virus (HPV) groups, as shown in Fig. 6A.
[b] Bold type signifies changes in gene expression induced by 1918(3P+NP)/K173 (|FC| ≥ 2) relative to K173.
[c] Underlining signifies changes in gene expression induced by HPV (|FC| ≥ 1.5) relative to 1918(3P+NP)/K173.

conjugates (41). Previous studies demonstrated that USP18 negatively regulates the innate immune responses (42). Uchida et al. demonstrated that USP18 gene was strongly expressed in chickens infected with lethal doses of highly pathogenic H5N1 influenza viruses, suggesting the correlation between USP18 expression level and the survival of the infected animals (43). In our study, however, the USP18 gene was highly expressed in the 1918(3P+NP)/K173 virus-infected mice as well as the high-pathogenicity group, suggesting that expression of USP18 gene may be associated with high viral growth in mouse lungs but not with the survival of the infected animals.

The threat of emergence of novel influenza viruses with pan-

demic potential is ever present, as demonstrated by the recent 2009 pandemic H1N1 influenza virus. To minimize the impact of future influenza pandemics, it is critical to understand the viral determinants that differentiate pandemic viruses from seasonal human influenza viruses, as well as the molecular mechanisms of the host response to highly pathogenic pandemic influenza viruses, in particular, the 1918 virus. Our data suggest that the 1918 virus HA and RNA polymerase genes contribute to efficient replication of viruses in mouse lungs; however, only the HA gene is responsible for lethality in mice. We have found that 1918 and 1918HA/K173 viruses induce similar host responses that are escalated and sustained from early acute infection and that T lymphocyte and NK cell responses distinguishing 1918 from 1918HA/K173 virus differ in magnitude, where 1918HA/K173 virus induces the same genes, though not to the same extent as the 1918 virus. This could account for differences in the clinical disease, such as morbidity and mortality, between the two highly pathogenic viruses. A deeper understanding of the cellular pathways impacted by 1918 virus HA and the molecular determinants in the viral glycoprotein that trigger this detrimental host response will aid in the development of immunomodulatory therapeutics to assist in the defense against future pandemic strains.

ACKNOWLEDGMENTS

We thank Kyoko Shinya for pathological analyses. We thank Martha McGregor, Kelly Moore, and Jean Chang for technical support. We also thank Peter Wilker and Ryo Takano for helpful discussions. We thank Susan Watson and Sarah Belisle for editing the manuscript.

This work was supported by National Institute of Allergy and Infectious Diseases Public Health Service research grants, by a Grant-in-Aid for Specially Promoted Research, by the Japan Initiative for Global Research Network on Infectious Diseases from the Ministry of Education, Culture, Sports, Science, and Technology, and by grants-in-aid from the Ministry of Health and by ERATO (Japan Science and Technology Agency).

REFERENCES

1. **Taubenberger JK, Reid AH, Janczewski TA, Fanning TG.** 2001. Integrating historical, clinical and molecular genetic data in order to explain the origin and virulence of the 1918 Spanish influenza virus. Philos. Trans. R. Soc. Lond. B Biol. Sci. **356**:1829–1839.
2. **Johnson NP, Mueller J.** 2002. Updating the accounts: global mortality of the 1918–1920 "Spanish" influenza pandemic. Bull. Hist. Med. **76**:105–115.
3. **Patterson KD, Pyle GF.** 1991. The geography and mortality of the 1918 influenza pandemic. Bull. Hist. Med. **65**:4–21.
4. **Simonsen L, Clarke MJ, Schonberger LB, Arden NH, Cox NJ, Fukuda K.** 1998. Pandemic versus epidemic influenza mortality: a pattern of changing age distribution. J. Infect. Dis. **178**:53–60.
5. **Grist NR.** 1979. Pandemic influenza 1918. Br. Med. J. **2**:1632–1633.
6. **Hewer CL.** 1979. 1918 influenza epidemic. Br. Med. J. **1**:199.
7. **Taubenberger JK, Morens DM.** 2008. The pathology of influenza virus infections. Annu. Rev. Pathol. **3**:499–522.
8. **Tumpey TM, Basler CF, Aguilar PV, Zeng H, Solorzano A, Swayne DE, Cox NJ, Katz JM, Taubenberger JK, Palese P, Garcia-Sastre A.** 2005. Characterization of the reconstructed 1918 Spanish influenza pandemic virus. Science **310**:77–80.
9. **Kobasa D, Jones SM, Shinya K, Kash JC, Copps J, Ebihara H, Hatta Y, Kim JH, Halfmann P, Hatta M, Feldmann F, Alimonti JB, Fernando L, Li Y, Katze MG, Feldmann H, Kawaoka Y.** 2007. Aberrant innate immune response in lethal infection of macaques with the 1918 influenza virus. Nature **445**:319–323.
10. **Kobasa D, Takada A, Shinya K, Hatta M, Halfmann P, Theriault S, Suzuki H, Nishimura H, Mitamura K, Sugaya N, Usui T, Murata T, Maeda Y, Watanabe S, Suresh M, Suzuki T, Suzuki Y, Feldmann H, Kawaoka Y.** 2004. Enhanced virulence of influenza A viruses with the haemagglutinin of the 1918 pandemic virus. Nature **431**:703–707.
11. **Pappas C, Aguilar PV, Basler CF, Solorzano A, Zeng H, Perrone LA, Palese P, Garcia-Sastre A, Katz JM, Tumpey TM.** 2008. Single gene reassortants identify a critical role for PB1, HA, and NA in the high virulence of the 1918 pandemic influenza virus. Proc. Natl. Acad. Sci. U. S. A. **105**:3064–3069.
12. **Tumpey TM, Garcia-Sastre A, Taubenberger JK, Palese P, Swayne DE, Basler CF.** 2004. Pathogenicity and immunogenicity of influenza viruses with genes from the 1918 pandemic virus. Proc. Natl. Acad. Sci. U. S. A. **101**:3166–3171.
13. **Hatta M, Gao P, Halfmann P, Kawaoka Y.** 2001. Molecular basis for high virulence of Hong Kong H5N1 influenza A viruses. Science **293**:1840–1842.
14. **Hatta M, Hatta Y, Kim JH, Watanabe S, Shinya K, Nguyen T, Lien PS, Le QM, Kawaoka Y.** 2007. Growth of H5N1 influenza A viruses in the upper respiratory tracts of mice. PLoS Pathog. **3**:1374–1379.
15. **Subbarao EK, London W, Murphy BR.** 1993. A single amino acid in the PB2 gene of influenza A virus is a determinant of host range. J. Virol. **67**:1761–1764.
16. **Neumann G, Watanabe T, Ito H, Watanabe S, Goto H, Gao P, Hughes M, Perez DR, Donis R, Hoffmann E, Hobom G, Kawaoka Y.** 1999. Generation of influenza A viruses entirely from cloned cDNAs. Proc. Natl. Acad. Sci. U. S. A. **96**:9345–9350.
17. **Reed LJ, Muench H.** 1938. A simple method of estimating fifty percent end points. Am. J. Hyg. **27**:493–497.
18. **Zornetzer GA, Frieman MB, Rosenzweig E, Korth MJ, Page C, Baric RS, Katze MG.** 2010. Transcriptomic analysis reveals a mechanism for a prefibrotic phenotype in STAT1 knockout mice during severe acute respiratory syndrome coronavirus infection. J. Virol. **84**:11297–11309.
19. **Smyth GK.** 2005. Limma: linear models for microarray data. Springer, New York, NY.
20. **Noth S, Brysbaert G, Benecke A.** 2006. Normalization using weighted negative second order exponential error functions (NeONORM) provides robustness against asymmetries in comparative transcriptome profiles and avoids false calls. Genomics Proteomics Bioinformatics **4**:90–109.
21. **Tchitchek N, Dzib J, Targat B, Noth S, Benecke A, Lesne A.** 2012. CDS: a fold-change based statistical test for concomitant identification of distinctness and similarity in gene expression analysis. Genomics Proteomics Bioinformatics **10**:127–135.
22. **Becavin C, Tchitchek N, Mintsa-Eya C, Lesne A, Benecke A.** 2011. Improving the efficiency of multidimensional scaling in the analysis of high-dimensional data using singular value decomposition. Bioinformatics **27**:1413–1421.
23. **Cox TF, Cox MAA.** 2000. Multidimensional scaling, 2nd ed. Chapman and Hall/CRC, Boca Raton, FL.
24. **Barrett T, Troup DB, Wilhite SE, Ledoux P, Evangelista C, Kim IF, Tomashevsky M, Marshall KA, Phillippy KH, Sherman PM, Muertter RN, Holko M, Ayanbule O, Yefanov A, Soboleva A.** 2011. NCBI GEO: archive for functional genomics data sets—10 years on. Nucleic Acids Res. **39**:D1005–D1010. doi:10.1093/nar/gkq1184.
25. **Kash JC, Basler CF, Garcia-Sastre A, Carter V, Billharz R, Swayne DE, Przygodzki RM, Taubenberger JK, Katze MG, Tumpey TM.** 2004. Global host immune response: pathogenesis and transcriptional profiling of type A influenza viruses expressing the hemagglutinin and neuraminidase genes from the 1918 pandemic virus. J. Virol. **78**:9499–9511.
26. **Kash JC, Tumpey TM, Proll SC, Carter V, Perwitasari O, Thomas MJ, Basler CF, Palese P, Taubenberger JK, Garcia-Sastre A, Swayne DE, Katze MG.** 2006. Genomic analysis of increased host immune and cell death responses induced by 1918 influenza virus. Nature **443**:578–581.
27. **Abdul-Careem MF, Mian MF, Yue G, Gillgrass A, Chenoweth MJ, Barra NG, Chew MV, Chan T, Al-Garawi AA, Jordana M, Ashkar AA.** 2012. Critical role of natural killer cells in lung immunopathology during influenza infection in mice. J. Infect. Dis. **206**:167–177.
28. **Perrone LA, Plowden JK, Garcia-Sastre A, Katz JM, Tumpey TM.** 2008. H5N1 and 1918 pandemic influenza virus infection results in early and excessive infiltration of macrophages and neutrophils in the lungs of mice. PLoS Pathog. **4**:e1000115. doi:10.1371/journal.ppat.1000115.
29. **Gaczynska M, Rock KL, Spies T, Goldberg AL.** 1994. Peptidase activities of proteasomes are differentially regulated by the major histocompatibility complex-encoded genes for LMP2 and LMP7. Proc. Natl. Acad. Sci. U. S. A. **91**:9213–9217.
30. **Rock KL, York IA, Saric T, Goldberg AL.** 2002. Protein degradation and the generation of MHC class I-presented peptides. Adv. Immunol. **80**:1–70.

31. **Pommerenke C, Wilk E, Srivastava B, Schulze A, Novoselova N, Geffers R, Schughart K.** 2012. Global transcriptome analysis in influenza-infected mouse lungs reveals the kinetics of innate and adaptive host immune responses. PLoS One **7**:e41169. doi:10.1371/journal.pone.0041169.
32. **Belisle SE, Tisoncik JR, Korth MJ, Carter VS, Proll SC, Swayne DE, Pantin-Jackwood M, Tumpey TM, Katze MG.** 2010. Genomic profiling of tumor necrosis factor alpha (TNF-alpha) receptor and interleukin-1 receptor knockout mice reveals a link between TNF-alpha signaling and increased severity of 1918 pandemic influenza virus infection. J. Virol. **84**:12576–12588.
33. **Basler CF, Reid AH, Dybing JK, Janczewski TA, Fanning TG, Zheng H, Salvatore M, Perdue ML, Swayne DE, Garcia-Sastre A, Palese P, Taubenberger JK.** 2001. Sequence of the 1918 pandemic influenza virus nonstructural gene (NS) segment and characterization of recombinant viruses bearing the 1918 NS genes. Proc. Natl. Acad. Sci. U. S. A. **98**:2746–2751.
34. **Billharz R, Zeng H, Proll SC, Korth MJ, Lederer S, Albrecht R, Goodman AG, Rosenzweig E, Tumpey TM, Garcia-Sastre A, Katze MG.** 2009. The NS1 protein of the 1918 pandemic influenza virus blocks host interferon and lipid metabolism pathways. J. Virol. **83**:10557–10570.
35. **Benecke A, Gale M Jr, Katze MG.** 2012. Dynamics of innate immunity are key to chronic immune activation in AIDS. Curr. Opin. HIV AIDS **7**:79–85.
36. **Chang ST, Tchitchek N, Ghosh D, Benecke A, Katze MG.** 2011. A chemokine gene expression signature derived from meta-analysis predicts the pathogenicity of viral respiratory infections. BMC Syst. Biol. **5**:202.
37. Katze MG (ed). 2012. Systems biology, vol 363. Springer, New York, NY.
38. **Boehm U, Klamp T, Groot M, Howard JC.** 1997. Cellular responses to interferon-gamma. Annu. Rev. Immunol. **15**:749–795.
39. **Schroder K, Hertzog PJ, Ravasi T, Hume DA.** 2004. Interferon-gamma: an overview of signals, mechanisms and functions. J. Leukoc. Biol. **75**:163–189.
40. **Wiley JA, Cerwenka A, Harkema JR, Dutton RW, Harmsen AG.** 2001. Production of interferon-gamma by influenza hemagglutinin-specific CD8 effector T cells influences the development of pulmonary immunopathology. Am. J. Pathol. **158**:119–130.
41. **Malakhov MP, Malakhova OA, Kim KI, Ritchie KJ, Zhang DE.** 2002. UBP43 (USP18) specifically removes ISG15 from conjugated proteins. J. Biol. Chem. **277**:9976–9981.
42. **Jeon YJ, Yoo HM, Chung CH.** 2010. ISG15 and immune diseases. Biochim. Biophys. Acta **1802**:485–496.
43. **Uchida Y, Watanabe C, Takemae N, Hayashi T, Oka T, Ito T, Saito T.** 2012. Identification of host genes linked with the survivability of chickens infected with recombinant viruses possessing H5N1 surface antigens from a highly pathogenic avian influenza virus. J. Virol. **86**:2686–2695.
44. **Bécavin C, Benecke A.** 2011. New dimensionality reduction methods for the representation of high dimensional 'omics' data. Expert Rev. Mol. Diagn. **11**:27–34.